

Article

Research on Path Tracking for an Orchard Mowing Robot Based on Cascaded Model Predictive Control and Anti-Slip Drive Control

Jun Li ^{1,2} , Sifan Wang ¹, Wenyu Zhang ¹, Haomin Li ¹, Ye Zeng ¹, Tao Wang ¹, Ke Fei ¹, Xinrui Qiu ¹, Runpeng Jiang ¹, Chaodong Mai ¹ and Yachao Cao ^{1,*}

¹ College of Engineering, South China Agricultural University, Guangzhou 510642, China; autojunli@scau.edu.cn (J.L.)

² Guangdong Laboratory for Lingnan Modern Agriculture, Guangzhou 510642, China

* Correspondence: yccaoryan@scau.edu.cn; Tel.: +86-020-8528-0632

Abstract: In complex orchard environments, orchard mowing robots are prone to longitudinal slippage because of the characteristics of tires and the adhesion conditions of the road surface, which makes it difficult for the robots to maintain high-precision path tracking and autonomous navigation positioning. This not only affects the accuracy of path tracking but also leads to unstable motion for the mowing robots. To solve the above problems, we take an orchard mowing robot as the control object and establish a cascaded path-tracking controller and an adaptive time domain model based on a kinematics model. By designing a linear error model, an objective function, and constraint conditions for the mowing robot, the optimal linear velocity and angular velocity of the mower are obtained and converted into the speed of the driving wheel. Then, an anti-slip driving controller is designed based on fuzzy control of the slip rate. The slip-rate-based fuzzy controller is constructed according to the real-time speed of the mower and the reference speed of the driving wheel solved by the model predictive controller, and anti-slip driving control is implemented through a combination of a PID controller and a tire dynamics model. To verify the effectiveness of the proposed method, simulation and field experiments are conducted. The experimental results show that the slip rate of the driving wheel of the mower remains within the target slip rate range in the orchard working environment, avoiding excessive driving wheel sliding. Furthermore, the average lateral error of the path-tracking controller is controlled within 0.05 m, and the average value of the longitudinal error is kept within 0.04 m, which satisfies the control accuracy requirements of lawn mower operations. The proposed method provides a reference optimization scheme for improving the path-tracking and motion stability of a mowing robot.

Keywords: mowing robot; path tracking; model predictive control; fuzzy control; slip rate



Citation: Li, J.; Wang, S.; Zhang, W.; Li, H.; Zeng, Y.; Wang, T.; Fei, K.; Qiu, X.; Jiang, R.; Mai, C.; et al. Research on Path Tracking for an Orchard Mowing Robot Based on Cascaded Model Predictive Control and Anti-Slip Drive Control. *Agronomy* **2023**, *13*, 1395. <https://doi.org/10.3390/agronomy13051395>

Academic Editors: Xiaoli Zhang, Dengsheng Lu, Xiujuan Chai, Guijun Yang and Langning Huo

Received: 15 April 2023

Revised: 13 May 2023

Accepted: 14 May 2023

Published: 18 May 2023



Copyright: © 2023 by the authors. Licensee MDPI, Basel, Switzerland. This article is an open access article distributed under the terms and conditions of the Creative Commons Attribution (CC BY) license (<https://creativecommons.org/licenses/by/4.0/>).

1. Introduction

Weeds pose a significant threat to the growth of fruit trees and affect the growth of fruit in orchards. Orchard weeding is an important part of fruit production, and mowing machinery can be used to effectively remove weeds and promote fruit tree production. Traditional weeding machinery has a large manual workload and high labor intensity and requires large amounts of manpower, funds, and time, seriously affecting the large-scale development of orchards [1]. In recent years, unmanned lawn-mowing robots have emerged and have become widely used. With their flexible motion modes and precise navigation and positioning systems, they have been widely used in work environments with simple terrain, effectively reducing labor costs and labor intensity [2]. However, the robot is affected by the complex orchard environment, which makes it easy for it to slip and pitch, as well as making it prone to other difficulties. During orchard operations, the posture of the mowing robot fluctuates greatly because of many interference factors.

Therefore, it is necessary to solve the problem of mowing robots having difficulty carrying out autonomous operations and maintaining path tracking smoothly.

Safe operations and path tracking are the core research issues related to unmanned lawn-mowing robots. Among them, control algorithms directly affect the stable operation of lawn-mowing robots and the accuracy of automatic navigation and positioning systems, thereby affecting the efficiency of lawn-mowing and fruit tree production. In recent years, scholars have conducted extensive research on the work efficiency, continuous and stable operation, and path-tracking control of unmanned agricultural machinery in complex operating environments, mainly using model predictive control (MPC), fuzzy control, pure tracking control, PID control, and linear quadratic regulator (LQR) control [3–10]. Yangyang [11] proposed an agricultural machine path-tracking algorithm based on optimal target points. Compared with the Pure Pursuit algorithm, the tracking error is reduced by more than 20%, and the tracking accuracy is significantly improved. Chenyuan Sun [12] proposed a distributed-drive agricultural vehicle based on multi-information fusion, in which the torque required by the wheels is distributed through a sliding mode control and incremental proportional integral control so that the total traction coefficient of each wheel is consistent, and the vehicle runs in a straight line to solve the problem of excessive wheel sliding, but the accuracy of path tracking is not solved.

However, these algorithms generally ignore the kinematics of agricultural machinery during driving and the dynamic constraints of the vehicle body. Model predictive control can establish corresponding models for special problems, consider multiple system constraints, predict future times, and conduct rolling optimization online in real time. Numerous studies have shown that the MPC algorithm is well suited for path-tracking problems with high real-time requirements, high accuracy requirements, and multi-input/output system constraints [13,14]. Guohai Liu [15] built a path-tracking controller and a self-tuning controller based on the kinematic model of a four-wheel independent-drive high-clearance spray. The model predictive controller was used as the main controller to achieve path-tracking control so that the lateral deviation of the spray could be controlled within 0.0141 m. Jiahong Xu [16] focused on the operational efficiency of agricultural machinery and proposed a new efficiency-oriented model predictive control (EfiMPC)-based path-tracking control algorithm to achieve optimal control and further improve the operational efficiency of agricultural machinery. Manikandan Sundaram [17] proposed an improved curve perception MPC (C-MPC) algorithm for navigating curved paths; their approach can effectively eliminate path noise on terrain such as farmland and has low horizontal and vertical errors. Jie He [18] established a kinematic model based on modifying the position and pose of agricultural machinery to obtain a linear error model, an objective function, and constraint conditions for agricultural machinery to perform path tracking, aiming at the sideration and skidding of agricultural machinery in a complex paddy field environment. The agricultural machinery body was taken as the control object, and the agricultural machinery position and pose were taken as the observation values. The average root-mean-square error of the three-line path-tracking result was 0.043 m, and the average absolute error was 0.033 m. Huang [19] proposed an integrated kinematics and dynamics model for unmanned vehicles, proposed a path-tracking controller based on MPC, and conducted a VE-DYNA-Simmink cosimulation under different speeds and road friction coefficients. The results showed that the algorithm has good tracking performance. Linhe Ge [20] designed an offset-free MPC solver that uses MPC to directly solve longitudinal and transverse coupling problems. Simulation results showed that the algorithm could attain better tracking accuracy and high-speed stability by considering longitudinal and transverse coupling constraints. The average time required to complete all computations was only 5 ms.

In summary, a path-tracking algorithm based on MPC can effectively solve the problems of agricultural machinery in navigation and path tracking, but it does not solve the problem of the driving wheel skidding in the orchard environment. In this paper, a cascade path-tracking control method for orchard mowing robots is designed, which is based on

the linear time-varying kinematic model of a four-wheel mower. The fixed time domain is difficult to adapt to the complex orchard environment, and to solve that problem, an adaptive time domain model predictive controller is designed. Aiming at the complex and varied road conditions of the orchard, a driving anti-skid controller was constructed using fuzzy control and the PID algorithm to realize driving anti-skid control. The proposed method improved the stability and the path-tracking accuracy of an orchard mowing robot.

2. Materials and Methods

2.1. Test Materials

To test the proposed path-tracking control method for an orchard mowing robot based on cascaded MPC and anti-skid drive control, the four-wheel differential mowing robot developed by the National Lychee and Longan Industrial Technology System Team of South China Agricultural University, which is mainly composed of a driving system, mowing system, and control system, is used as the experimental platform. The mowing system is connected to the body through an electric push rod, and the stubble-height CAN is adjusted through the electric push rod. The MPC controller is connected to the lower machine controller through the CAN port, which coordinates with the rotary coding sensor to control the motion of the mower. Figure 1 shows the mowing robot prototype. Table 1 shows the main technical parameters of the mowing robot.

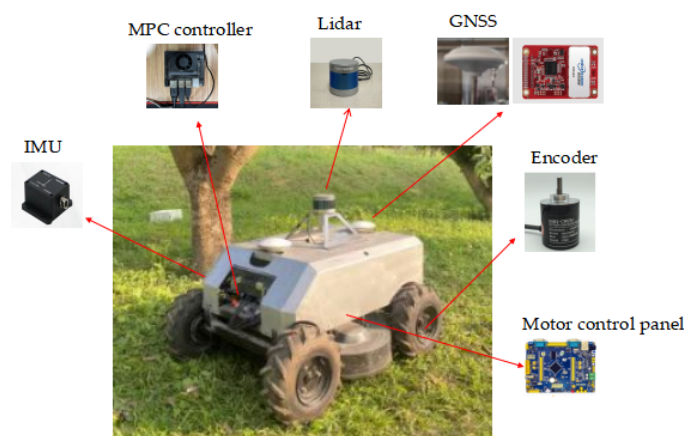


Figure 1. Lawn mower and sensors.

Table 1. Main technical parameters of the lawn mower.

Technical Parameters	Parameters
Length × width × height	1051 × 831 × 460 (mm)
Wheel track (<i>B</i>)	593 (mm)
Wheelbase (<i>L</i>)	715 (mm)
Working speed	0–1.5 (m/s)
Drive form	Four-wheel independent drive
Communication interface	CAN
Mowing robot quality	70 ± 1 (kg)
Wheel radius	165 (mm)
Rated motor power	350 (W)
Maximum motor speed	1500 (rad/min)

The position, attitude (heading angle, pitch angle, and roll angle), angular velocity, acceleration, and traveling speed of the mowing robot are measured using GPS, an IMU, and a wheeled odometer, as shown in Figure 1. The IMU sensor is installed horizontally forward inside the body shell, GPS antennas are installed in pairs on the roof, and the encoder is installed coaxially with the motor. The static measurement accuracy of the IMU sensor is 0.05°, the dynamic measurement accuracy is 0.1°, and the maximum output

frequency is 400 Hz. During testing, the update frequency of the IMU is set to 50 Hz, and that of the GPS is set to 10 Hz.

The speed of the four wheels of the mowing robot is measured by an OMRON photoelectric encoder, as shown in Figure 1. The resolution of the adopted encoder is 2000 pulse/rotation (P/R), and the sampling period of the wheel speed is set to 20 ms for testing.

2.2. Experimental Methods

2.2.1. Method Design for Measuring the Slip Rate of a Mowing Robot

In the orchard environment, the running speed of the mowing robot and the motion path are set as shown in Figure 2. Through autonomous navigation, the starting point and ending point of the mowing robot are set, its real-time speed and the real-time speed of the four wheels in the motion path are recorded, and the real-time slip rate of the mowing robot is obtained under the working state according to the real-time speed of the mowing robot and the motor speed.

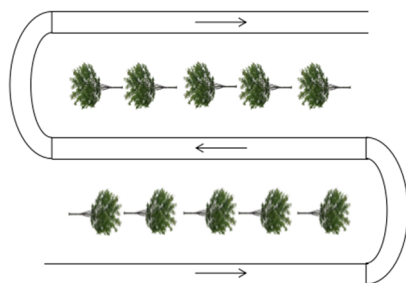


Figure 2. Schematic diagram of the reference path.

2.2.2. Path-Tracking Parameter Definition

To verify the effectiveness of the control method proposed in the following section, a four-wheel differential lawn mower platform is used to perform a path-tracking experiment and a slide rate control experiment in a standard orchard at South China Agricultural University. According to the actual situation of the orchard, the operation route of the lawn mower adopts a full coverage path. At the same time, to ensure that the simulation path is consistent with the actual working path of the lawn mower, the standard orchard is measured. The distance of each straight path is approximately 25 m, and the turning path is approximately 10 m.

Path tracking requires not only the state quantity of the lawn mower itself but also the corresponding reference path, which consists of information such as the position and attitude tracked by the lawn mower. Before building the control system, the reference path needs to be defined, as shown in Figure 2. Navigation equipment can provide effective positioning data, mainly using the longitude, L ; latitude, B ; and heading angle, φ . The reference path is generally composed of discrete reference waypoints, whose coordinates are longitudes and latitudes (L, B, φ) in the WGS-84 coordinate system. It is necessary to first convert these coordinates to the geodetic coordinate system (the Gauss–Kruger projection method is adopted) [21] and then to the body plane coordinate system [13], and the reference path obtained after transformation is used as the simulation reference path in MATLAB.

3. Mower Path-Tracking Controller Design Based on Adaptive MPC and Slip-Rate-Based Fuzzy Control

3.1. Four-Wheel Differential Kinematic Model of the Lawn Mower

Regarding the wheeled lawn mower platform, the motor can drive the wheels and change the wheel speeds independently. Therefore, the essence of path tracking for the lawn mower is to adjust the torque of each wheel in real time. The torque outputs of different wheels control the motor, allowing the speeds of the lawn mower in different

directions to be generated to realize straight running and steering for the lawn mower. Because the mower uses differential steering, in which the left and right wheels of the mower run at different speeds, the mower is able to turn. Therefore, the geometric center of the robot is taken as the origin of the coordinate system of the lawn mower, and c denotes the instantaneous center of the lawn mower's steering. A kinematic model of the lawn mower is developed in Figure 3.

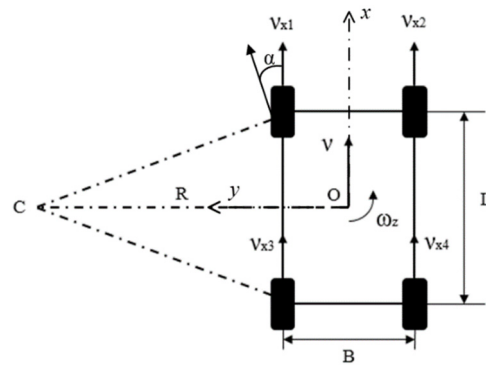


Figure 3. Kinematic model of a four-wheel differential-speed lawn mower.

Taking the forward direction of the lawn mower body as the x -axis, the rotation axis is perpendicular to the vehicle and upward, and the counterclockwise direction is specified as forward rotation without considering the lateral motion of the body, ω ($i = 1, 2, 3, 4$), or the rotational speeds of the four wheels, namely, the motor speed; v is the translational speed of the mower along the x -axis, and θ is the angular velocity of the geometric center of the mower. The angle between the actual velocity of the tire and the orientation of the tire is the tire sideslip angle.

After completing the corresponding matrix transformation, the state equation of a four-wheel independent-drive lawn mower can be derived, as shown in Equation (1):

$$\begin{pmatrix} \dot{x} \\ \dot{y} \\ \dot{\theta} \end{pmatrix} = \begin{pmatrix} \cos\theta & 0 \\ \sin\theta & 0 \\ 0 & 1 \end{pmatrix} \begin{pmatrix} v \\ \omega \end{pmatrix} = \begin{pmatrix} \frac{r}{4}\cos\theta & \frac{r}{4}\cos\theta & \frac{r}{4}\cos\theta & \frac{r}{4}\cos\theta \\ \frac{r}{4}\sin\theta & \frac{r}{4}\sin\theta & \frac{r}{4}\sin\theta & \frac{r}{4}\sin\theta \\ -\frac{r}{2B} & -\frac{r}{2B} & -\frac{r}{2B} & -\frac{r}{2B} \end{pmatrix} \begin{pmatrix} \omega_1 \\ \omega_2 \\ \omega_3 \\ \omega_4 \end{pmatrix} \tag{1}$$

$$= \begin{pmatrix} \frac{1}{4}\cos\theta & \frac{1}{4}\cos\theta & \frac{1}{4}\cos\theta & \frac{1}{4}\cos\theta \\ \frac{1}{4}\sin\theta & \frac{1}{4}\sin\theta & \frac{1}{4}\sin\theta & \frac{1}{4}\sin\theta \\ -\frac{1}{2B} & -\frac{1}{2B} & -\frac{1}{2B} & -\frac{1}{2B} \end{pmatrix} \begin{pmatrix} v_1 \\ v_2 \\ v_3 \\ v_4 \end{pmatrix}$$

where ω_i ($i = 1, 2, 3, 4$) refers to the wheel angular velocity, r is the wheel radius of the lawn mower, v_i ($i = 1, 2, 3, 4$) is the wheel edge line velocity, B is the track width, and ω and v are the angular velocity and linear velocity of the geometric center of the lawn mower, respectively.

As shown in Equation (1), the motion state of a four-wheel independent-drive lawn mower in the x - and y -axis directions is described, and the components, angular velocity, and wheel rotation angular velocity of the lawn mower travel speed along the x and y coordinate axes are determined, ω_i ($i = 1, 2, 3, 4$), producing the relationship between the wheel edge velocities, v_i ($i = 1, 2, 3, 4$).

3.2. Design of an Adaptive Time Domain Model of a Predictive Controller

3.2.1. Linear Error Discretization of the Kinematic Lawn Mower Model

According to the state equation shown in Equation (1), the system can be regarded as an input with $u = (v, \omega)^T$, and the state variables are $\chi = (x, y, \theta)^T$. The general form of the linear control system of T is shown in Equation (2) [14]. The heading angle of the

lawn mower, θ , is equal to the angle between the geometric center of the lawn mower and the x -axis.

$$\dot{\chi} = f(\chi, u) \tag{2}$$

If the working path of the mower acquired based on GPS is taken as the reference path and each path point on the reference path satisfies the established kinematic equation, then a kinematic model that satisfies the preset conditions is shown in Equation (3):

$$\dot{\chi}_r = f(\chi_r, u_r) \tag{3}$$

where $\chi_r = (x_r, y_r, \theta_r)^T, u_r = (v_r, \omega_r)^T$.

By expanding the above equation using Taylor’s formula at the first reference point of the reference path [20] and ignoring higher-order terms, the linear error model of the lawn mower is obtained, as shown in Equation (4):

$$\dot{\chi} = f(\chi_r, u_r) + \left. \frac{\partial f(\chi, u)}{\partial \chi} \right|_{\substack{\chi = \chi_r \\ u = u_r}} (\chi - \chi_r) + \left. \frac{\partial f(\chi, u)}{\partial u} \right|_{\substack{\chi = \chi_r \\ u = u_r}} (u - u_r) \tag{4}$$

The linearized error model of the lawn mower can be calculated by combining the above two equations:

$$\dot{\tilde{\chi}} = \begin{pmatrix} \dot{x} - \dot{x}_r \\ \dot{y} - \dot{y}_r \\ \dot{\theta} - \dot{\theta}_r \end{pmatrix} = A \begin{pmatrix} x - x_r \\ y - y_r \\ \theta - \theta_r \end{pmatrix} = A + B \begin{pmatrix} v - v_r \\ \omega - \omega_r \end{pmatrix} \tag{5}$$

In the equation, A and B are the Jacobian matrices of f with respect to x and u , respectively; $A = \begin{pmatrix} 0 & 0 & -v_r \sin \theta_r \\ 0 & 0 & v_r \cos \theta_r \\ 0 & 0 & 0 \end{pmatrix}$, and $B = \begin{pmatrix} \cos \theta_r & 0 \\ \sin \theta_r & 0 \\ 0 & 1 \end{pmatrix}$.

To apply the linearization error model to the MPC controller, discretization processing is performed by the forward Euler method [22] to obtain the linear error discretization model of the system, as shown in the following equation:

$$\begin{cases} \tilde{\chi}(k+1) = A_{k,t} \tilde{\chi}(k) + B_{k,t} \tilde{u}(k) \\ y(k) = C_{k,t} \tilde{\chi}(k) \end{cases} \tag{6}$$

where $A_{k,t} = \begin{pmatrix} 1 & 0 & -v_r \sin \theta_r \cdot T \\ 0 & 1 & v_r \cos \theta_r \cdot T \\ 0 & 0 & 1 \end{pmatrix}, B_{k,t} = \begin{pmatrix} \cos \theta_r \cdot T & 0 \\ \sin \theta_r \cdot T & 0 \\ 0 & T \end{pmatrix}, C_{k,t} = \begin{pmatrix} 1 & 0 & 0 \\ 0 & 1 & 0 \\ 0 & 0 & 1 \end{pmatrix}$, and T is the sampling time.

3.2.2. Design of the Objective Function and Constraint Conditions

To prevent the control variables in the system from experiencing sudden changes, which may lead to decreases in the path-tracking accuracy and system stability of the lawn mower, control increments are used to replace the control variables. The modified state equation is as follows:

$$\tilde{\zeta}(k|t) = \begin{pmatrix} \tilde{\chi}(k|t) \\ \tilde{u}(k-1|t) \end{pmatrix} \tag{7}$$

Therefore, the output state quantity of the system can be expressed as follows:

$$\eta(k) = \tilde{c}_{k,t} \tilde{\zeta}(k|t) \tag{8}$$

where $\eta(x, y, \theta)^T$ represents the output of the discrete MPC system, x represents the horizontal axis position of the lawn mower, y represents the vertical axis position (m) of the lawn mower, and θ represents the heading angle of the lawn mower in degrees.

After modification, the state equation used for the MPC controller is represented as follows:

$$\begin{cases} \zeta(k+1) = \tilde{A}\zeta(k) + \tilde{B}\Delta u(k) \\ \eta(k) = \tilde{c}_{k,t}\zeta(k|t) \end{cases} \tag{9}$$

where $\Delta u(k) = \tilde{u}(k) - \tilde{u}(k-1)$, $\tilde{A}_{k,t} = \begin{pmatrix} A_{k,t} & B_{k,t} \\ 0_{m \times n} & I_m \end{pmatrix}$, $\tilde{B}_{k,t} = \begin{pmatrix} B_{k,t} \\ I_m \end{pmatrix}$, $\tilde{c}_{k,t} = \begin{bmatrix} k_1 & 0 & 0 & 0 & 0 \\ 0 & k_2 & 0 & 0 & 0 \\ 0 & 0 & k_3 & 0 & 0 \end{bmatrix}$,

and n represents the dimensionality of the system state variable. In this article, n is equal to 3, m is the dimensionality of the control variable, and m is 2. k_1, k_2 , and k_3 are the weight ratios of the three state variables' errors.

The modified state prediction equation is iteratively derived, and the system's prediction output is set as follows:

$$Y(k+1|k) = f_{\zeta}\zeta(k) + f_u\Delta U(k) \tag{10}$$

where Y is the output matrix of the system, ΔU is the control increment matrix, f_{ζ}

and f_u are the iterative matrices of the equation, $Y(k+1|k) = \begin{bmatrix} \eta(k+1|k) \\ \eta(k+2|k) \\ \dots \\ \eta(k+N_p|k) \end{bmatrix}$, $f_{\zeta} =$

$$\begin{bmatrix} \tilde{C}_k \tilde{A}_k \\ \tilde{C}_k \tilde{A}_k^2 \\ \dots \\ \tilde{C}_k \tilde{A}_k^{N_p} \end{bmatrix}, \Delta U(k) = \begin{bmatrix} \Delta u(k|k) \\ \Delta u(k+1|k) \\ \dots \\ \Delta u(k+N_c|k) \end{bmatrix}, \text{ and } f_u = \begin{bmatrix} \tilde{C}_k \tilde{B}_k & 0 & \dots & 0 \\ \tilde{C}_k \tilde{A}_k \tilde{B}_k & \tilde{C}_k \tilde{B}_k & \dots & 0 \\ \vdots & \vdots & \ddots & \vdots \\ \tilde{C}_k \tilde{A}_k^{N_p-1} \tilde{B}_k & \tilde{C}_k \tilde{A}_k^{N_p-2} \tilde{B}_k & \dots & \tilde{C}_k \tilde{A}_k^{N_p-N_c-1} \tilde{B}_k \end{bmatrix}.$$

Considering the actual working situation of the lawn mower, when designing the MPC controller, the control quantity and control increment constraints are considered, which is beneficial for improving the path-tracking accuracy of the lawn mower. The design of the objective function mainly revolves around the deviation of the system state variables and the constraints of the control variables during the operation of the lawn mower. A multi-objective optimization function is designed with constraints based on the control objective proposed earlier, and the objective function for the control is predicted using the following model form:

$$J(k) = \sum_{i=1}^{N_p} \|\eta(k+i|k) - \eta_{ref}(k+i|k)\|_Q^2 + \sum_{i=1}^{N_c-1} \|\Delta U(k+i|k)\|_R^2 + \rho \varepsilon^2 \tag{11}$$

where N_p is the predictive time domain; N_c is the control time domain; ΔU is the control increment in the control time domain; ε is the relaxation factor; Q is the weight matrix of the output quantity; R is the weight matrix of the control increment; ρ is the weight matrix of the relaxation factor; $\eta_{ref}(X_{ref}, Y_{ref}, \theta_{ref})$ is the reference output variable; and η_{ref} is the global reference path for the working environment of the lawn mower.

To prevent the problem of variables being unsolvable during the solving process, a relaxation factor, ε , and a weight matrix representing the relaxation factor, ρ , need to be added. In the objective function, it is necessary to calculate the output of the system in the predicted time domain.

In the optimization objective function, the solution is the control time domain. The control increment within N_c can only appear in the form of a control increment or its multiplication with the transformation matrix with the constraint conditions applied. Therefore, it is necessary to transform the control increment constraint inequality and obtain the corresponding transformation matrix.

$$U_{min} \leq U_t + A\Delta U_t \leq U_{max} \tag{12}$$

$$A = \begin{bmatrix} 1 & 0 & \cdots & \cdots & 0 \\ 1 & 1 & 0 & \cdots & 0 \\ 1 & 1 & 1 & \ddots & 0 \\ \vdots & \vdots & \ddots & \ddots & \vdots \\ 1 & 1 & \cdots & 1 & 1 \end{bmatrix} \tag{13}$$

In the formula, U_{\max} and U_{\min} refer to the control time domain. The sum of the maximum and minimum values of the control variables is within N_c ; A is the coefficient matrix, and $A \otimes I_m$. Here, \otimes is the Kronecker product, and I_m is the m-dimensional identity matrix.

In the model predictive control system proposed in this article, constraints can be set to better reflect physical facts, and MPC has the advantage of allowing its constraints to be modified online, whereas other optimization methods do not. According to the principles of control algorithms and the physical structure of the chassis, the constraints in this article mainly include the control limit constraints and control increment constraints during the control process. The constraint conditions are as follows [3]:

$$u_i(k+j) \leq u(k+j) \leq u_a(k+j), j = 0, 1, \dots, N_c - 1 \tag{14}$$

$$\Delta u_i(k+j) \leq \Delta u(k+j) \leq \Delta u_a(k+j), j = 0, 1, \dots, N_c - 1 \tag{15}$$

where u_i and u_a represent the minimum and maximum values of the control variables, respectively, and Δu_i and Δu_a represent the minimum and maximum values of the control increment, respectively.

3.2.3. Optimization Problem-Solving

To solve the above optimization problem by using quadratic programming, it is necessary to convert the objective function into the following standard form:

$$\min J = \frac{1}{2} Z^T Q Z + C^T Z \tag{16}$$

After integrating the objective function and constraints, the controller needs to output control sequences to the system during each control cycle, convert the objective function into a standard quadratic form, and incorporate the constraints to solve the following optimization problems:

$$J(\xi(k), u(k-1), \Delta U(k)) = [\Delta U(k)]^T \varepsilon^T H_k [\Delta U(k)^T, \varepsilon] + G_k [\Delta U(k)^t, \varepsilon] \tag{17}$$

$$s.t. \Delta U_{\min} \leq \Delta U(k) \leq \Delta U_{\max} \tag{18}$$

$$U_{\min} \leq U_t + A \Delta U(k) \leq U_{\max} \tag{19}$$

where $H_k = \begin{pmatrix} f_{uk}^T Q f_{uk}^T & 0 \\ 0 & \rho \end{pmatrix}$, $G_k = [2E(k)^T Q f_{uk} \quad 0]$, and $E(k)$ denotes the tracking errors in the predicted time domain.

The system solves the standard quadratic form combined with constraints in each control cycle and obtains the control sequence in the control time domain. According to the basic theory of MPC, the first element, $\Delta u(k)$, in the control sequence is applied to the system as the actual control quantity, as shown in Equation (20):

$$\tilde{u}(k) = \bar{u}(k-1) + \Delta u(k) \tag{20}$$

When the system repeats the above optimization process after each control cycle until the entire control process is completed, tracking control is achieved for the reference path of the mowing robot.

3.2.4. Adaptive Time Domain Module Design

The time-domain parameters of model predictive control have a significant impact on the control effect, but fixed parameters have poor adaptability to complex operating conditions and cannot adapt to the environment in real time. Among them, the two parameters with the most significant impacts are the control time domain and the prediction time domain.

As shown in Figure 4, when the other control parameters remain unchanged, the larger the prediction time domain is, the larger the range predicted by the controller, which can obtain more lawn mower state information. However, if the prediction time domain is too large, it will increase the error of the lawn mower at a distant position, thereby reducing the tracking accuracy of the lawn mower at a nearby position [23]. In addition, an excessively large prediction time domain will also increase the computational complexity of the MPC algorithm and reduce the real-time performance of the system [24]. When the prediction time domain is too small, the status information of the lawn mower will decrease. In the presence of system control constraints, the lawn mower will be unable to turn in a timely manner, the path-tracking accuracy will be reduced, and stability will not be ensured.

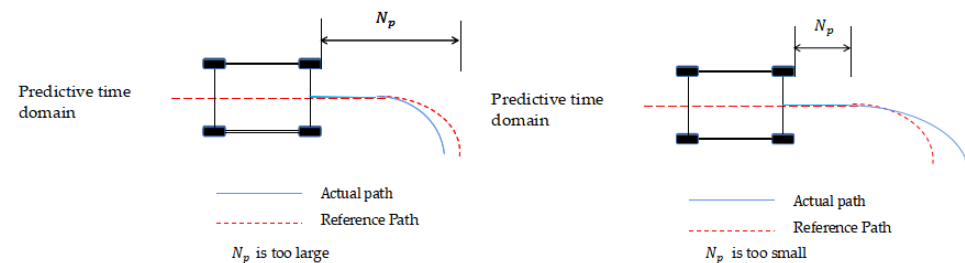


Figure 4. Analysis of the impact under different N_p conditions.

Based on the model predictive controller set above, in this section, a control time domain and prediction time domain optimization module is designed based on the vehicle's speed, as shown in Figure 5, to achieve adaptive parameter adjustment, improve the adaptability of the mower to environmental changes, and improve the path-tracking accuracy of the mower.

As the vehicle speed increases, the distance predicted by the MPC controller also needs to increase accordingly; that is, the predicted time domain, N_p , increases accordingly to ensure the stable tracking of the reference path by the lawn mower and to avoid the untimely turning phenomenon. For the control time domain, N_c , an increase in N_c can reduce the degree of sudden change in the control quantity and prevent the vehicle from slipping or even losing control during high-speed driving [25]. Therefore, the control time domain should also increase appropriately with increasing vehicle speed to ensure the stability of path tracking.

As shown in the Figure 5, a time domain optimization module based on vehicle speed is designed using a fuzzy control algorithm. The design input is the current speed of the lawn mower, and the predicted time domain is the output. Based on the motor performance of the lawn mower, the input walking speed range of the lawn mower is determined to be $[0, 0.8 \text{ m/s}]$, and the adaptive predicted time domain value range for the reference path combined with the control algorithm is $[10, 30]$.

The speed and prediction time domain of the lawn mower is divided into the following seven fuzzy subsets: NB (very small), NM (small), NS (small), Z (moderate), PS (large), PM (large), and PB (large). The membership function selects the Gaussian and trigonometric functions.

Based on the time domain optimization design and multiple simulation experiments, specific fuzzy rules are formulated, as shown in Table 2. The response relationship between the operating speed of the lawn mower and the predicted time domain is shown in Figure 6. The operating speed of the lawn mower is obtained through fuzzy inference to determine

the predicted fuzzy output in the time domain. The centroid method is selected to solve the ambiguity of this problem and obtain an accurate output prediction in the time domain.

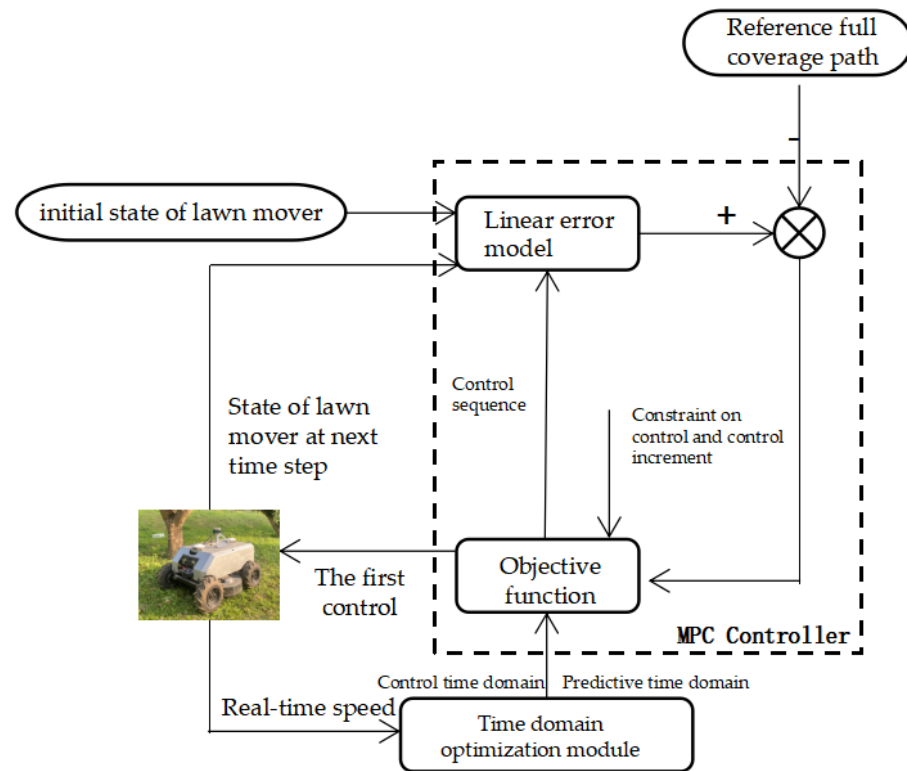


Figure 5. Block diagram of the adaptive time domain MPC path-tracking control process.

Table 2. Fuzzy rule table.

Fuzzy Quantity	Fuzzy Subset
v	NB NM NS Z PS PM PB
N_p	NB NM NM Z PM PB PB

where v is the speed of the lawn mower, N_p is the predicted time domain.

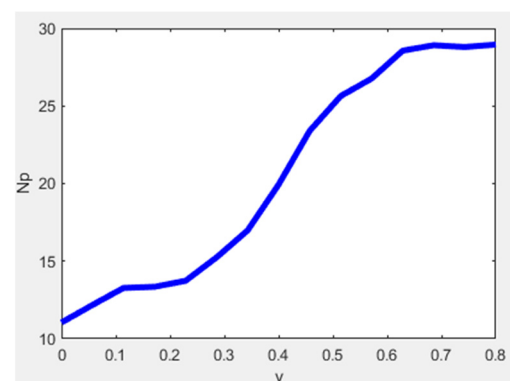


Figure 6. Response graph for the speed and prediction time domain.

The prediction time domain output is smoothed by the fuzzy algorithm to obtain the current optimal prediction time domain, N_{pb} , after fuzzy processing. The current optimal prediction time domain is appropriately adjusted to obtain the current optimal control time domain, N_{cb} . The expressions for N_{pb} and N_{cb} are as follows:

$$N_{pb} = Round(N_p) \tag{21}$$

$$N_{cb} = \text{Round}(\alpha * N_p) \quad (22)$$

In the above equation, α is a time domain weight parameter, which usually ranges from 0.15 to 0.2. Here, based on the simulation situation, the time domain weight coefficient is selected as 0.2.

3.3. Mower Driving Wheel Anti-Slip Control Based on Fuzzy Slip Rate Control

The driving wheel of a lawn mower may experience significant longitudinal slippage in complex operating environments, which can affect the path-tracking accuracy and stable operation of the mower. Therefore, it is necessary to consider the impact of driving wheel slippage on path-tracking accuracy.

3.3.1. Establishing a Dynamic Model for the Driving Wheel of a Mower

To analyze the state of the driving wheel of a lawn mower, a dynamic model is established; interference such as air resistance is ignored, as shown in Figure 7.

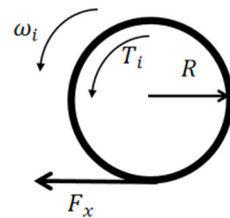


Figure 7. Dynamic model of the driving wheel of a lawn mower.

The dynamic equation for the driving force of the lawn mower is established as shown in Equation (22):

$$J\dot{\omega} = T_i - RF_x - T_x \quad (23)$$

Therefore, the torque of the driving wheel of the lawn mower can be expressed as follows:

$$T_i = J\dot{\omega} + RF_x + T_x \quad (24)$$

The rotational inertia of the driving wheel can be expressed as follows:

$$J = \frac{MR^2}{2} \quad (25)$$

where J is the moment of inertia (kg/m^2), ω is the angular acceleration of the driving wheel (rad/s^2), T_i is the torque of the driving wheel ($\text{N}\cdot\text{m}$), R is the radius of the driving wheel (m), F_x is the longitudinal driving force of the tire (N), T_x is the rolling resistance moment ($\text{N}\cdot\text{m}$), and M is the mass of the lawn mower (kg).

In this article, the standard Pacejka magic equation is used. The H.B. Pacejka tire model is an empirical model that fits actual test data. Its form is universal and can simultaneously describe the relationships between the longitudinal force of the tire and the longitudinal slip rate, the lateral force and the lateral tire angle, the return torque and the lateral tire angle, and the vertical wheel load. Moreover, its fitting accuracy is high, so it is called the “magic formula”. The magic formula includes the longitudinal tire force under single driving or braking conditions, the lateral tire force under single steering conditions, and the longitudinal tire force and the lateral force under combined drive/braking conditions [26,27].

Under a single driving/braking condition, the relationship between the longitudinal tire force, longitudinal slip rate, and vertical tire load can be described as follows:

$$F_{x0} = D_1 \sin\{C_1 \arctan[B_1 \lambda - E_1(B_1 \lambda - \arctan B_1 \lambda)]\} \quad (26)$$

where the curve form factor is $C_1 = 1.65$, the peak factor is $D_1 = a_1F_z^2 + a_2F_z$, $B_1C_1D_1 = (a_3F_z^2 + a_4F_z)e^{-a_5F_z}$, the stiffness factor is $B_1 = \frac{B_1C_1D_1}{C_1D_1}$, the curvature factor of the curve is $E_1 = a_6F_z^2 + a_7F_z + a_8$, λ is the longitudinal slip rate, and a_i is the fitting coefficient.

Under pure steering conditions, the relationship between the longitudinal tire force, F_{y0} ; the tire side deflection angle, α ; and the vertical tire load, F_z , can be described as follows:

$$F_{y0} = D_2 \sin\{C_2 \arctan[B_2x - E_2(B_2x - \arctan B_2x)]\} \tag{27}$$

$$x = \alpha + S_h \tag{28}$$

where the curve form factor is $C_2 = 1.3$; the peak factor is $D_2 = a_1F_z^2 + a_2F_z$; $B_2C_2D_2 = a_3 \sin[a_4 \arctan(a_5F_z)](1 - a_{12}|\gamma|)$; the stiffness factor is $B_2 = \frac{B_2C_2D_2}{C_2D_2}$; the horizontal drift of the curve is $S_h = a_9\gamma$; the vertical drift of the curve is $S_v = (a_{10}F_z^2 + a_{11}F_z)\gamma$; the curvature factor of the curve is $E_2 = a_6F_z^2 + a_7F_z + a_8$; α is the tire sideslip angle; and γ is the wheel camber angle [28].

The relationship between the longitudinal tire force, F_x , and lateral force, F_y , under the combined driving/braking and steering conditions, as well as the lateral tire slip angle, α , and longitudinal slip rate, λ , is as follows:

$$F_x = \frac{\sigma_x}{\sigma} F_{x0}, F_y = \frac{\sigma_y}{\sigma} F_{y0} \tag{29}$$

where $\sigma = \sqrt{\sigma_x^2 + \sigma_y^2}$, $\sigma_x = -\frac{\lambda}{1+\lambda}$, $\sigma_y = -\frac{\tan\alpha}{1+\lambda}$.

By referring to the traditional tire model and the attributes of the lawn mower itself, the above values can be assigned to determine the relationship between the longitudinal and lateral forces of the tire and the slip rate, as shown in Figure 8.

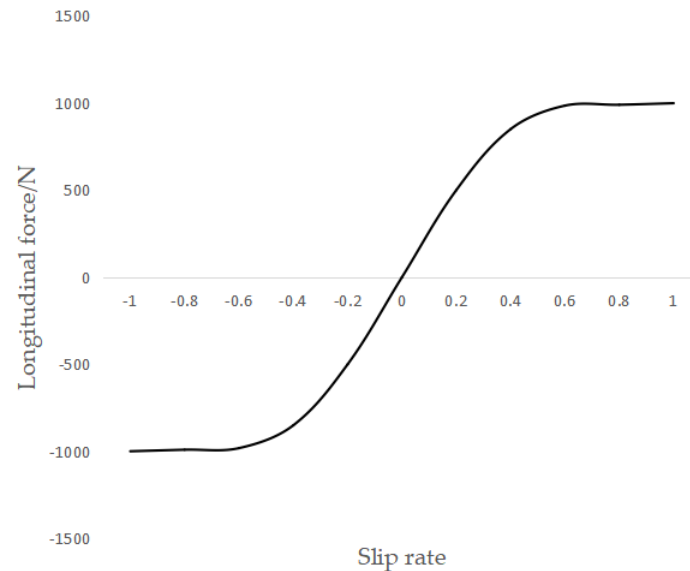


Figure 8. Diagram of the relationship between the longitudinal force and the slip rate.

3.3.2. Target Slip Rate Range of Lawn-Mowing Robots

The slip rate of the driving wheel is defined as the relative error between the wheel speed of the driving wheel and the absolute speed of the vehicle body [29]. In this article, the rotational speed data of the driving wheel are collected under the working condition of the lawn mower through pre-experiments, the real-time slip rate of the lawn mower during a certain working cycle is calculated according to Equation (29), and the target slip rate of the driving wheel is analyzed based on this. In general, whether wheel slippage

occurs is measured by the slip rate of the driving wheel. This article uses the following slip rate expression:

$$s = \frac{\omega r - v}{\max(\omega r, v)} \quad (30)$$

where ω is the angular velocity of rotation; v is the moving speed of the lawn mower; and R is the wheel radius. In this article, the radii of all wheels are assumed to be equal.

According to the design of the slip rate measurement experiment in Section 2.2.1, the lawn mower is controlled to perform repeated working experiments on the working path, recording the real-time speed and motor-related parameters of the lawn mower on this working path. The real-time slip rate of the lawn mower is calculated according to Equation (29), and the relationships between the motor parameters and slip rate are analyzed, as shown in the following figures.

Because of the use of a hub motor in the lawn mower in this article, the performance parameters of the motor can better reflect the states of the driving wheels. Based on the real-time speeds of the four driving wheel motors during the experiment, the effective output power and slip rate data of the motor are analyzed. From Figure 9, it can be observed that, when the slip rate is maintained within 0–0.2, the speed of the drive wheel motor is relatively stable, and the observed changes are roughly linear. When the slip rate exceeds 0.4, the speed of the drive wheel motor rapidly increases until the slip rate reaches approximately 0.9, and the motor speed of the drive wheel approaches the maximum speed. At this point, it can be determined that the drive wheel is idling. As shown in Figure 10, when the slip rate of the driving wheel is maintained below 0.2, the effective output power of the driving wheel motor remains in its optimal state. When the slip rate reaches approximately 0.9, the effective power of the driving wheel motor approaches 0, and at this time, the motor is not in operation, and the driving wheel is in an idle state. Based on the above analysis, the target slip rate in this article is not fixed to a certain value. The aim of the value condition is to first ensure that no slip occurs; that is, the target slip rate should be controlled within $[-0.2, 0.2]$. If it exceeds this range, the slip rate is controlled by a fuzzy controller to force it to lie within this range.

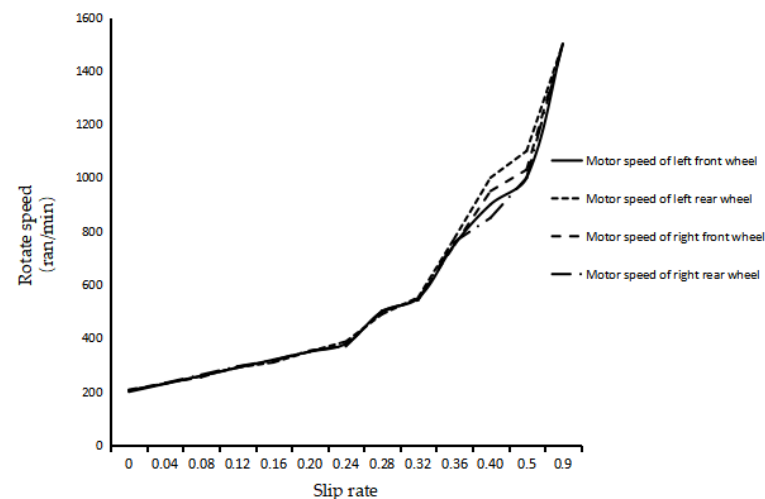


Figure 9. Relationship between the slip rate and real-time speed of the driving wheel.

3.3.3. Fuzzy Controller Design Considering the Slip Rate

This article adopts a dual-input single-output fuzzy control algorithm, where the inputs are the expected speed of the driving wheel obtained by the MPC controller and the real-time speed of the mower, and the output is the expected slip rate of the driving wheel of the mower. Based on the real-time vehicle speed feedback obtained from the lawn mower and the expected wheel speed of the MPC controller; the driving speed range of the lawn mower is set to $[-0.8 \text{ m/s}, 0.8 \text{ m/s}]$; the real-time speed range of the driving wheel is

set to $[-5 \text{ rad/s}, 5 \text{ rad/s}]$; and according to the previous analysis, the expected slip rate range is set to $[-0.2, 0.2]$.

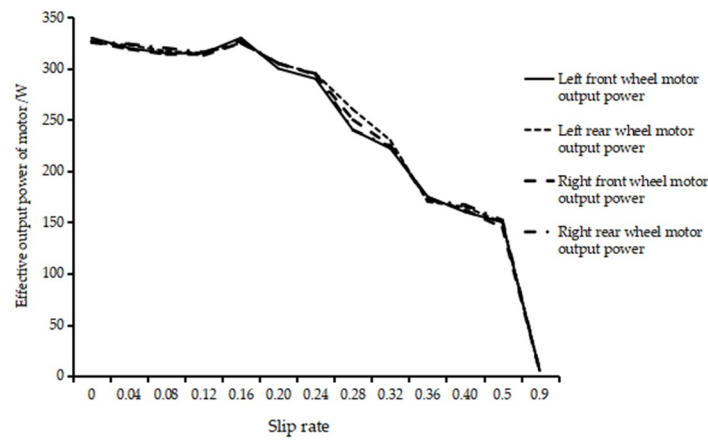


Figure 10. Diagram of the relationship between the slip rate and the effective output power of the drive wheel motor.

The reference speed, real-time drive wheel speed, and expected slip rate of the lawn mower are divided into the following seven fuzzy subsets: NB (very small), NM (small), NS (small), Z (moderate), PS (large), PM (large), and PB (large). In terms of membership function selection, the system adopts the combination of a Gaussian function and a trigonometric function, which not only ensures that the system has high sensitivity but also makes the system more stable.

Based on the relationships between the slip rate, vehicle speed, and driving wheel speed and after conducting many simulation experiments, the most common If–Then rule in fuzzy control is adopted. Specific fuzzy rules are formulated, as shown in Table 3. The response relationship between the reference speed of the lawn mower, the speed of the driving wheel, and the expected slip rate is shown in Figure 11. When one of the indicators of driving wheel speed and real-time speed changes, or both changes, the slip rate will be affected.

Table 3. Table of fuzzy slip rate control rules.

ω	v						
	NB	NM	NS	Z	PS	PM	PB
NB	Z	PB	PM	PM	PS	Z	Z
NM	PM	Z	PM	PS	PS	Z	NS
NS	PM	PM	Z	PS	Z	NS	NS
Z	NS	PM	PS	Z	NS	NM	NM
PS	NM	PS	NM	NS	Z	NM	NM
PM	NM	Z	NM	NM	NM	Z	NB
PB	NB	Z	NB	NM	NM	NB	Z

The reference driving wheel speed of the MPC controller and the speed of the lawn mower are input through fuzzy inference to obtain the fuzzy output. The centroid method is chosen to solve the ambiguity and obtain an accurate expected slip rate output.

This article adopts the classic incremental PID control method [30] for the design of the slip rate PID controller, whose expression is as follows:

$$u_s(k) = K_{ps} * e_s(k - 1) + K_{is} * e_s(k) + K_{ds} * (e_s(k) - 2e_s(k - 1) + e_s(k - 2)) + u_s(k - 1) \tag{31}$$

In the equation, $u_s(k)$ is the slip rate output by the lawn mower at this time, and $u_s(k - 1)$ is the last output quantity.

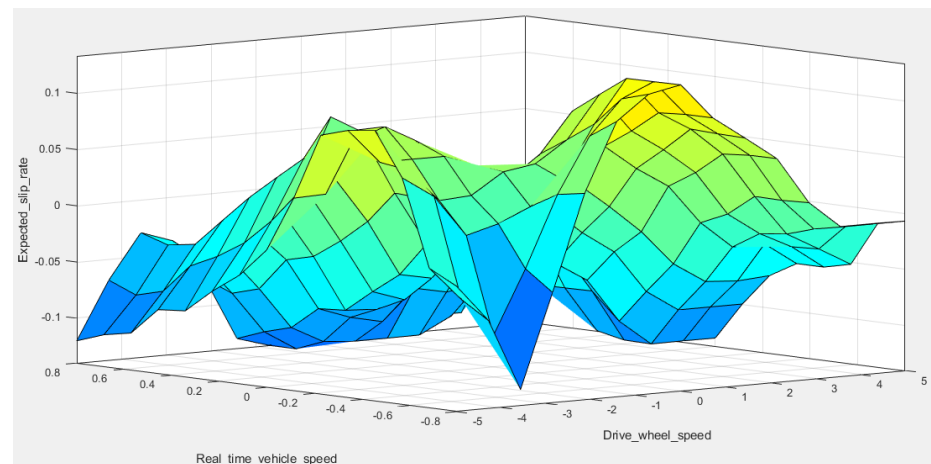


Figure 11. Diagram of the relationship between the driving wheel speed, real-time vehicle speed, and expected slip rate.

For the PID controller applied to the motor torque, incremental PID control is also used, and its expression is as follows:

$$u_v(k) = K_{pv} * e_v(k - 1) + K_{iv} * e_v(k) + K_{dv} * (e_v(k) - 2e_v(k - 1) + e_v(k - 2)) + u_v(k - 1) \tag{32}$$

In the equation, $u_v(k)$ is the current torque output by the drive motor of the lawn mower, and $u_v(k - 1)$ is the last output quantity. The slip rate and driving wheel torque of the PID controller are shown in Figure 12:

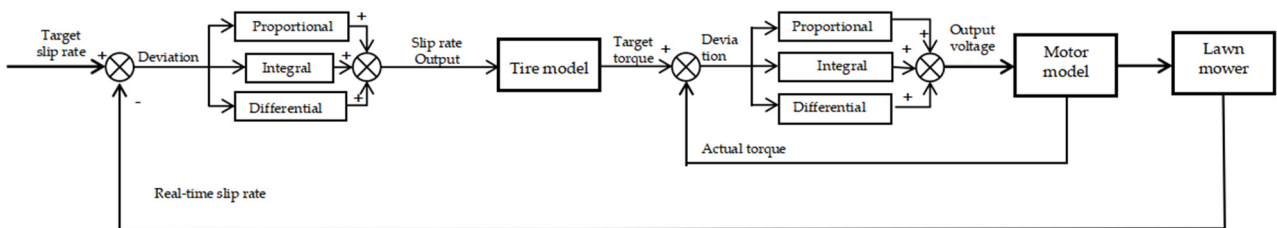


Figure 12. Incremental PID control chart for the slip rate and driving wheel torque.

Based on many simulation experiments and field experiments, the PID controller parameter values are set as shown in Table 4.

Table 4. Table of fuzzy slip rate control rules.

PID Controller Parameters	Value
Dwelling time/s	0.02
Proportional slip rate control	3
Integral slip rate control	1
Differential slip rate control	0.6
Proportional drive wheel motor speed control	5
Integral drive wheel motor speed control	1.6
Differential drive wheel motor speed control	0.8

In summary, the fuzzy control algorithm can obtain the expected slip rate of the driving wheel based on the fuzzy rule table formulated by the fuzzy controller, the target speed of the driving wheel obtained by the MPC controller, and the real-time speed fed back from the lawn mower. The PID controller of the slip rate is designed to control the expected slip rate obtained by the fuzzy controller and the actual measured slip rate and obtain the output slip rate of the driving wheel. By combining the dynamic model of the lawn mower with a torque PID controller, the torque of the motor is controlled to achieve anti-slip control for the lawn mower.

3.4. Path-Tracking Controller for Designing Adaptive MPC and Fuzzy Slip Rate Control Schemes

The path-tracking controller based on MPC and fuzzy control performs anti-slip control for the lawn mower by controlling the slip rate and torque of the driving wheels. The concrete implementation steps are shown in Figure 13. First, a dynamic model for the driving wheel of the lawn mower is established, the relationship between the slip rate and road adhesion coefficient is analyzed through the dynamic model, and the range of slip rates at which the driving wheel does not slip is obtained. Based on the MPC controller output of Section 3.2, the linear speed and angular velocity of the vehicle are obtained, and the expected driving wheel speed is determined through the use of a four-wheel differential steering model. Then, the expected slip rate is calculated by the real-time vehicle speed feedback derived from the actual process. If the observed rate is within the nonslip range, it is considered the target slip rate. If it exceeds the range, it is input into the established fuzzy controller to control the slip rate within a moderate range and output the target slip rate. A slip rate PID controller that outputs the target speed through real-time slip rate feedback obtained from the actual process to control the slip rate of the driving wheel near the target slip rate is designed. The target speed of the driving wheel obtained from the previous step is calculated with the target speed obtained from the MPC; it is converted into the final output slip rate, and the tire dynamics model is used for verification purposes. The real-time steering angle speed feedback from the actual process is used to obtain the lateral wheel angle. The slip rate, lateral angle, and vertical wheel load are substituted into the magic equation under the longitudinal and lateral joint working conditions to obtain the longitudinal force acting on the wheel, thereby obtaining the output torque of the target motor. A torque PID controller that combines real-time torque feedback from the motor with the output voltage is designed to control the torque. Finally, the torque output by the motor is input into the actual process, which can ensure that the wheel slip rate is within the nonslip range, guaranteeing that the driving wheel is in a better working state and achieving anti-slip control of the lawn mower driving wheel. The overall control diagram is as follows.

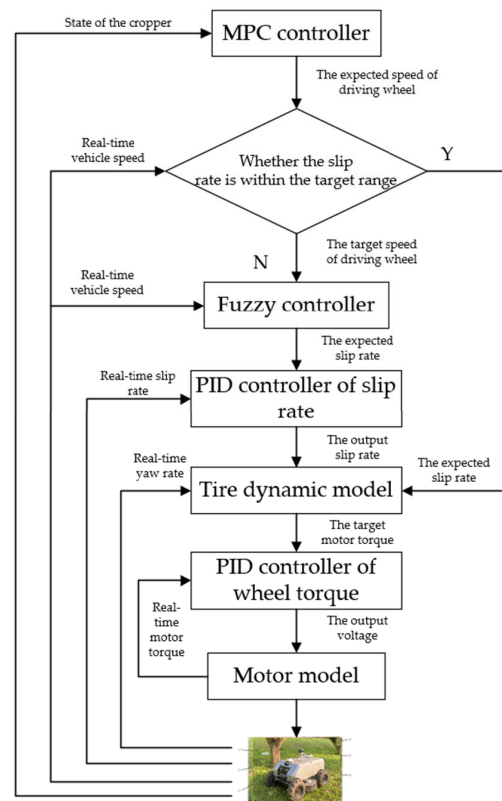


Figure 13. Path-tracking control system diagram for lawn mowers.

4. Results and Discussion

4.1. Path-Tracking Simulation

4.1.1. Adaptive MPC-Based Path-Tracking Simulation

An adaptive path-tracking simulation platform is built for lawn mowers based on MATLAB/Adams, and a flat road with an unchanged road adhesion coefficient is set in Adams. The path is a looping curve, and the MPC controller is implemented through S-FUSION. It can dynamically describe system changes and achieve variable conversion based on real-time system changes. The main simulation control diagram is shown in Figure 14.

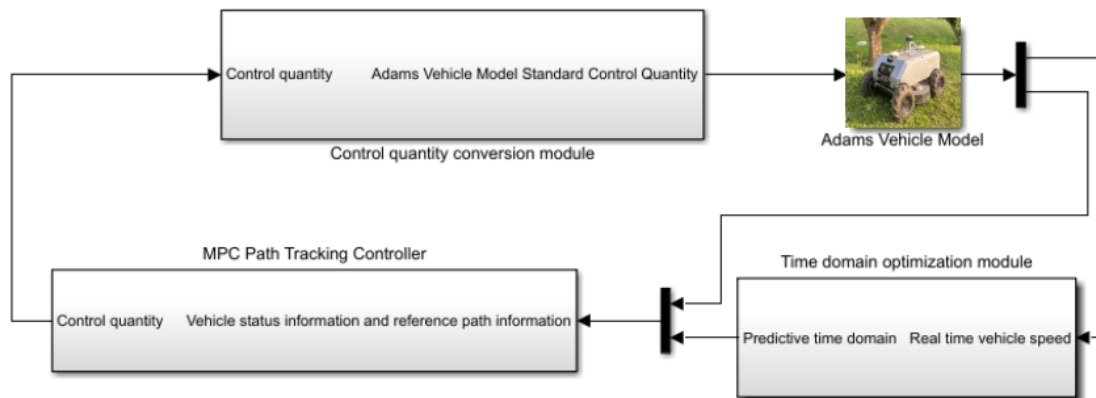


Figure 14. Structure diagram of the adaptive MPC simulation system.

The purpose of the controller is to accurately and quickly track the reference path while minimizing deviations and maintaining tracking stability during the tracking process. According to the controller design mentioned above, path-tracking control is performed by setting a fixed time domain parameter control group and a model predictive controller in the adaptive time domain for double-shift simulation experiments and loop path simulation experiments. The predicted time domain, Np , of the fixed time domain parameter control group is 15, and the control time domain, Nc , is 3. The constraints of the control quantity and control increment are shown in Equation (32), and the basic parameters of the model predictive controller are shown in Table 5.

$$\begin{cases} -0.8 \text{ m/s} \leq v \leq 0.8 \text{ m/s} \\ -0.2 \text{ rad/s} \leq \omega \leq 0.2 \text{ rad/s}' \end{cases} \begin{cases} -0.1 \text{ m/s} \leq \Delta v \leq 0.1 \text{ m/s} \\ -0.04 \text{ rad/s} \leq \Delta \omega \leq 0.04 \text{ rad/s} \end{cases} \quad (33)$$

Table 5. MPC controller parameter table.

Basic Parameters of the Model Predictive Controller	Numerical Value
Sampling time (s)	0.2
Reference speed (m/s)	0.6
Relaxation factor weight coefficient	10
Relaxation factor, ϵ	10
Weight matrix, Q	$\begin{bmatrix} 10 & \cdots & 0 \\ \vdots & \ddots & \vdots \\ 0 & \cdots & 10 \end{bmatrix}_{3N_p}$
Weight matrix, R	$\begin{bmatrix} 1 & \cdots & 0 \\ \vdots & \ddots & \vdots \\ 0 & \cdots & 1 \end{bmatrix}_{2N_c}$

The reference path is set to a looping path, and the simulation results are shown in Figure 15, and the relevant data are shown in Table 6. From the path-tracking effect, it can be seen that the fixed time domain controller does not fit the reference path as well as the

adaptive time domain controller at turns. From Figures 16 and 17, it can be concluded that the absolute value of the maximum lateral error in the fixed time domain is 0.13 m, the average value of the lateral error is 0.075 m, the absolute value of the maximum longitudinal error is 0.135 m, and the average value of the longitudinal error is 0.058 m. The absolute value of the maximum horizontal error in the adaptive time domain is 0.115 m, the average horizontal error is 0.043 m, the absolute value of the maximum vertical error is 0.085 m, and the average vertical error is 0.041 m. From the lateral and vertical deviations of the path, it can be observed that whether a fixed time domain or an adaptive time domain is utilized, the error is larger in places with larger turning angles. Overall, the adaptive time domain has a better effect on path tracking, with smaller errors.

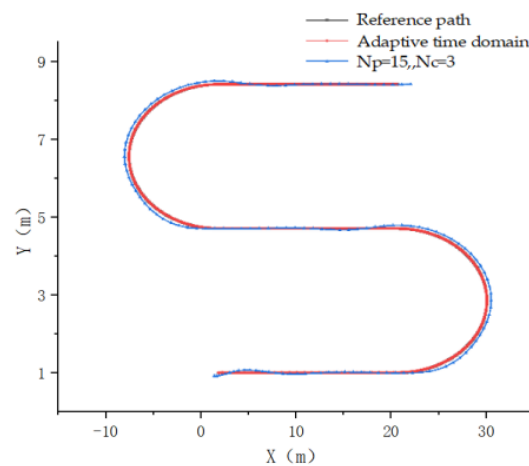


Figure 15. Effect diagram of looping path tracking.

Table 6. Comparison between the controller parameters of the fixed time domain and adaptive time domain.

Time Domain Parameters	$N_p = 15$ $N_c = 3$	Adaptive Time Domain Parameters
Absolute value of the maximum lateral error (m)	0.13	0.115
Average lateral error (m)	0.075	0.043
Absolute value of the maximum longitudinal error (m)	0.135	0.085
Mean value of the longitudinal error (m)	0.058	0.041

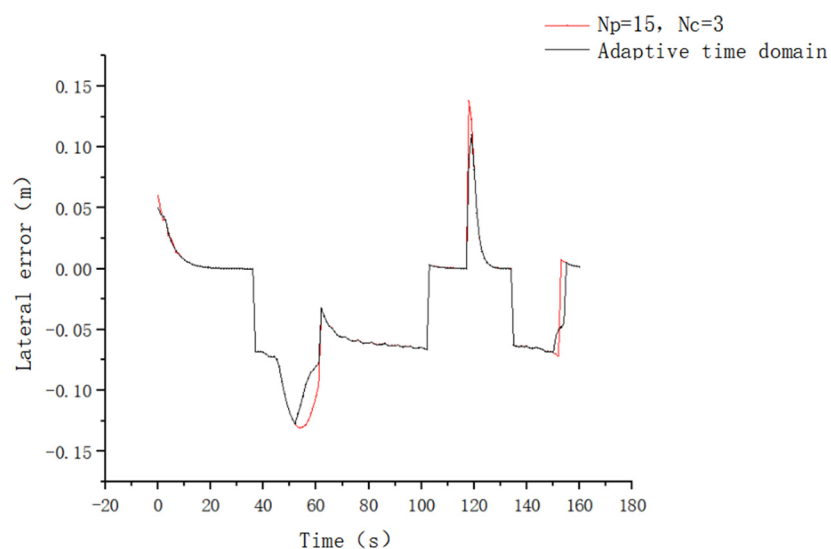


Figure 16. Lateral error results of the path simulation.

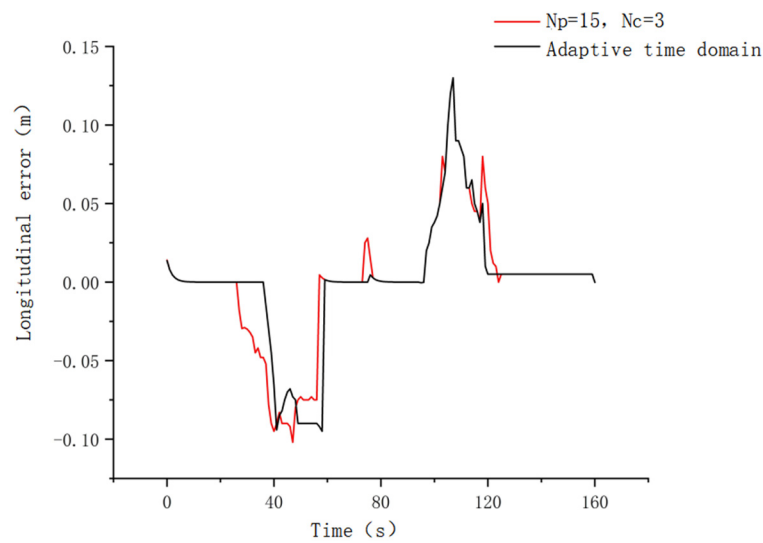


Figure 17. Longitudinal error results of the path simulation.

In summary, the adaptive time domain-based MPC controller performs better in terms of tracking the looping path than the fixed time domain-based MPC controller and can adapt to complex orchard environments.

4.1.2. Simulation Experiment Involving the Path-Tracking Controller Combined with Anti-Slip Drive Control

A predictive controller and a fuzzy controller are built for the slip rate of a lawn mower model based on MATLAB, and a joint simulation is conducted with the wheel mower model built using Adams. The simulation structure is shown in Figure 18.

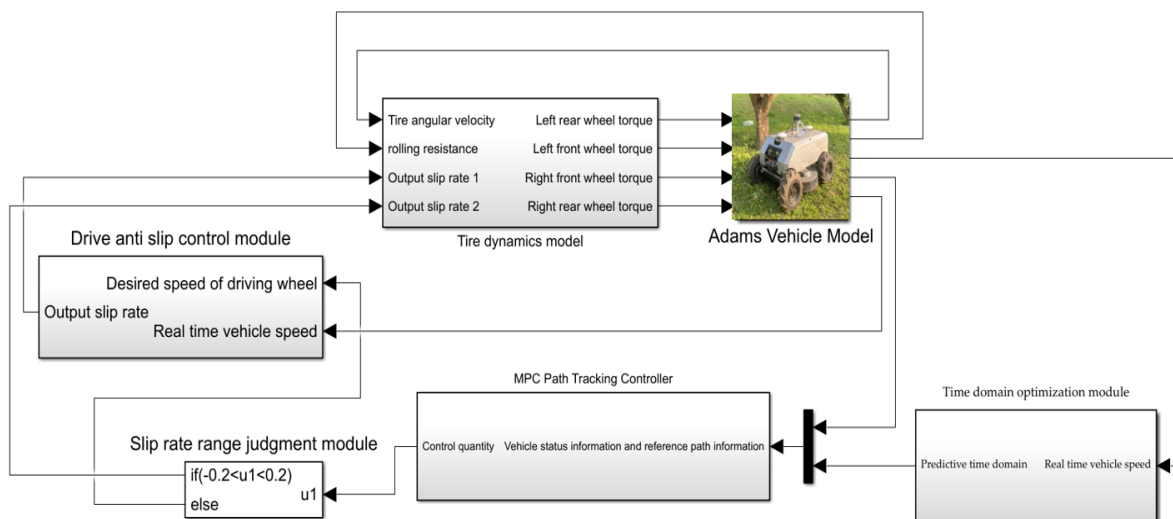


Figure 18. Simulation structure diagram of the combined anti-slip drive control and path-tracking control method.

Based on Adams’ random road surface design with varying road coefficients and reference paths, comparative simulation experiments are conducted on the path-tracking controller combined with anti-slip driving control and the MPC path-tracking control approach designed in this paper. Figures 19 and 20 show the slip rate variation curves of the front-left drive wheel and the front-right drive wheel, respectively. Figures 19 and 20 show that, during the operation of the lawn mower, because of changes in the road adhesion coefficient, the longitudinal driving force of the lawn mower is inconsistent, and the driving wheel experiences significant sliding. After adding a fuzzy controller based on the slip

rate, the slip rate of the lawn mower can be effectively controlled within the target slip rate range, indicating that, within this reference path and these road conditions, the slip rate of the driving wheel remains in a relatively good state, and the speed variation of the driving wheel is not high, resulting in good working performance. When the MPC controller without added anti-slip driving tracks the reference path, because of the change in the road adhesion coefficient, the slip rate changes significantly, with a maximum value close to 0.6. At this time, the lawn mower seriously slips, which has a significant impact on the resulting path-tracking accuracy. Therefore, the addition of a path-tracking controller with anti-slip driving ability has the effect of suppressing slip, and the path-tracking effect is better.

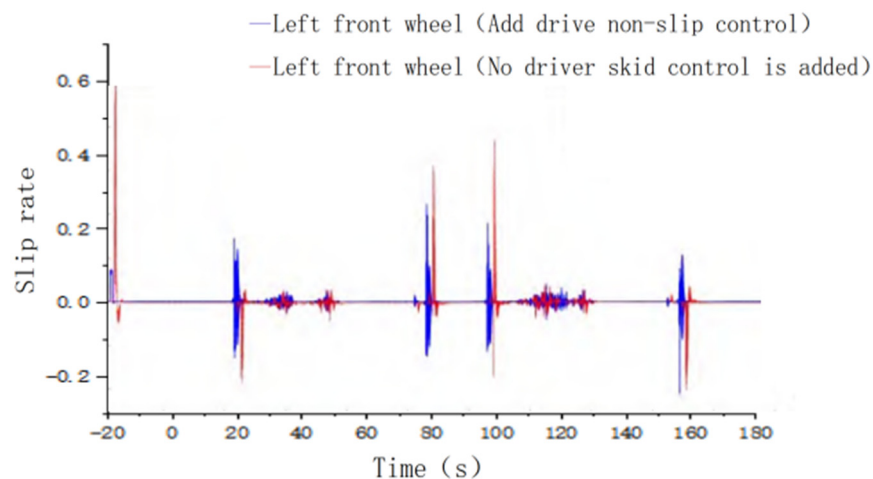


Figure 19. Comparison diagram concerning the slip rate of the left front wheel of the lawn mower.

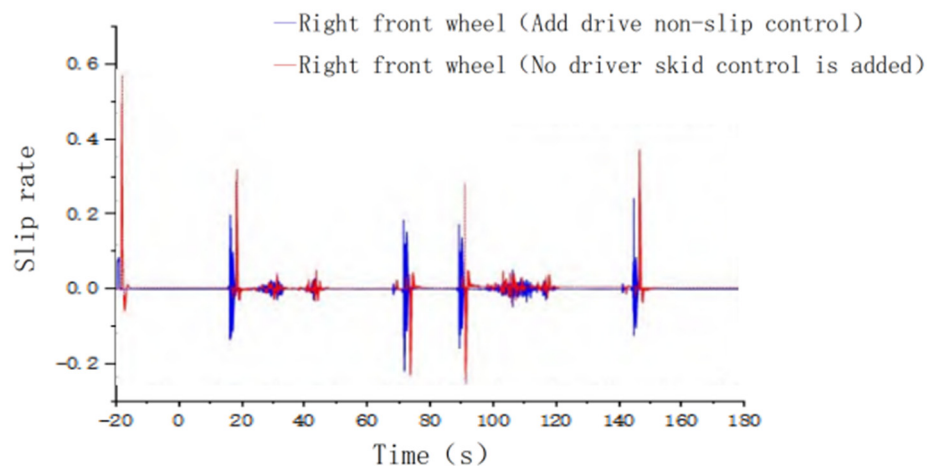


Figure 20. Comparison involving the slip rate of the right front wheel of the lawn mower.

As shown in Figure 21, compared with traditional MPC control, the MPC-based path-tracking controller with added anti-slip drive control fits the reference path better and can also effectively track the reference path in areas with larger turns.

4.2. Field Trial Verification

Utilizing the lawn-mowing robot platform built in Section 2.1, the fixed reference path set in Figure 2 is determined through the pre-experimental collection, and path-tracking control and anti-slip driving control experiments are performed for verification purposes. The upper computer automatically saves the lateral deviation data and the slip rate data of the driving wheels during the lawn mower working process and conducts statistical analyses on the data. The comparative effects of the slip rates of the four driving wheels

and the lateral and longitudinal path-tracking deviations are shown in the figure. For the convenience of analysis, the slip rate is taken as an absolute value.

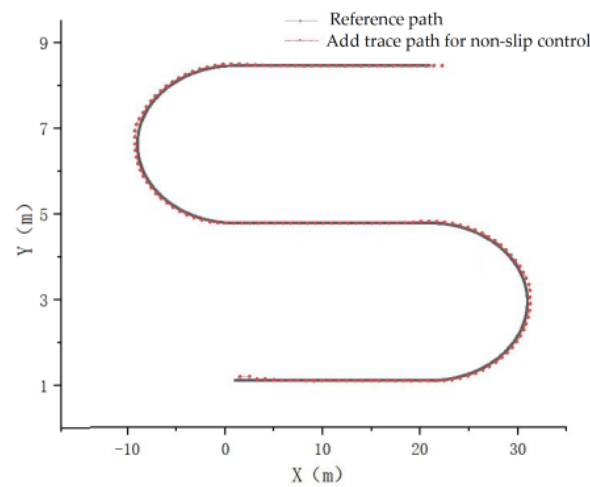


Figure 21. Diagram comparing the actual path and reference path under anti-slip drive control.

As shown in Figures 22–25, without the addition of an anti-slip drive controller, the amplitude of the slip rate change curve of the lawn mower is relatively large when driving on the reference path, with an amplitude of approximately 0.5. At this point, the different driving wheels experience varying degrees of slipping, seriously affecting the path-tracking effect. After adding an anti-slip controller to the driving wheel, the slip rate can be maintained within a range of 0–0.2. According to the pre-experimental results and the slip rate analysis in Section 3.3.2, the working state of each driving wheel is optimal at this slip rate. In summary, with the addition of an anti-slip drive controller, the absolute values of the slip rates of the four drive wheels can be maintained within the target slip rate range. At this time, the longitudinal adhesion coefficient of the road surface remains in a linear upward range, providing a larger and smoother longitudinal driving force, improving the stability of the lawn mower during autonomous operation, and reducing the working energy consumption of the lawn mower.

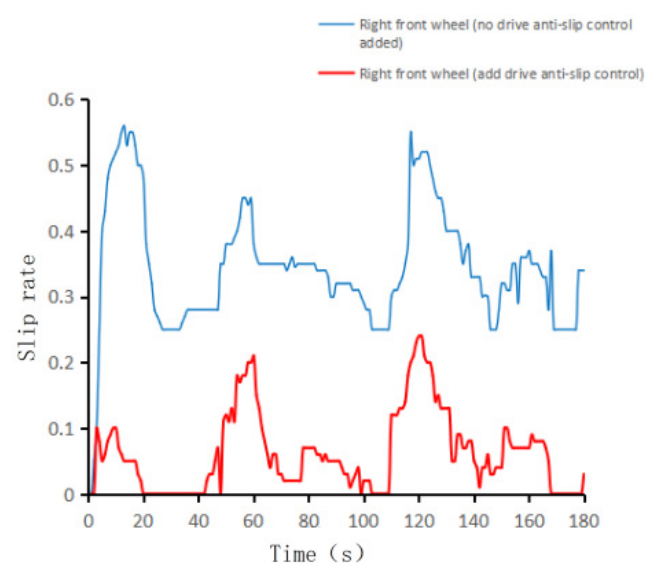


Figure 22. Comparison diagram concerning the slip rate of the front-right wheel.

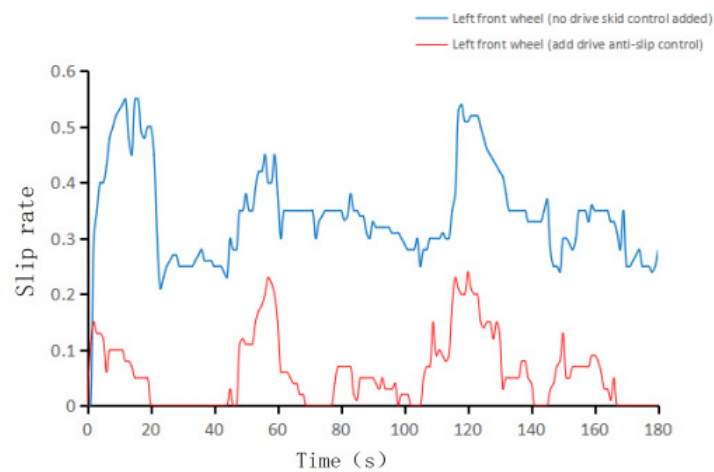


Figure 23. Comparison diagram concerning the slip rate of the front-left wheel.

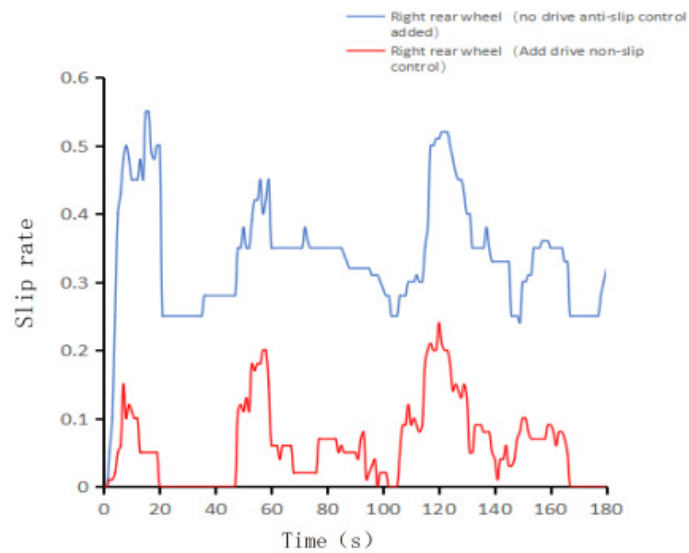


Figure 24. Comparison diagram showing the slip rate of the rear-right wheel.

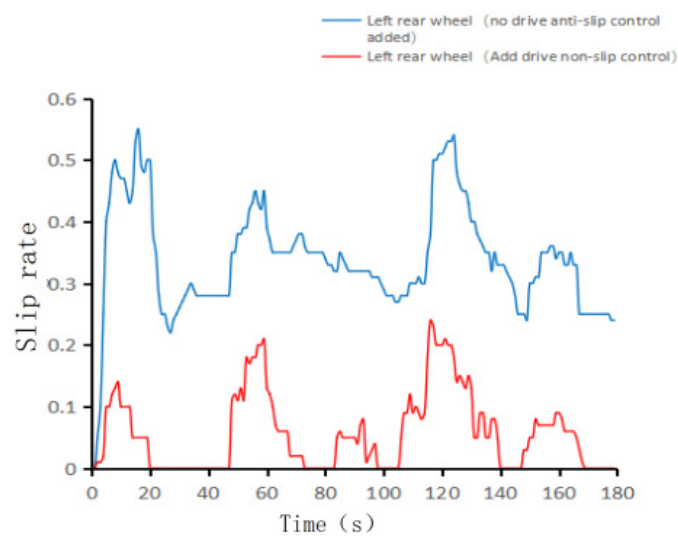


Figure 25. Comparison diagram involving the slip rate of the rear-left wheel.

During the experiment, actual path-tracking points are also collected and compared with the expected path points for data analysis purposes. The period for collecting the

experimental data is approximately 180 s after the lawn mower completes a full reference path (as shown in Figure 2), with a path length of approximately 95 m. The results in Figures 26 and 27 indicate that the average absolute values of the lateral errors of the path points can be controlled within 0.05 m, and the average absolute values of the longitudinal errors can be controlled within 0.04 m.

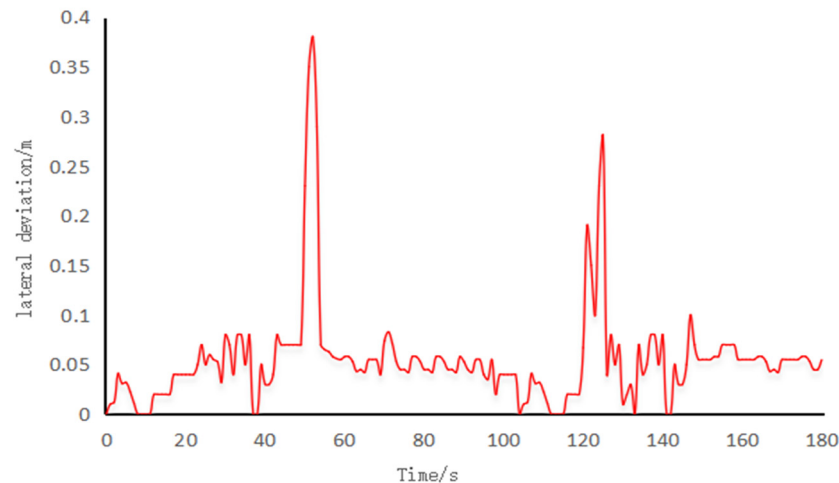


Figure 26. Lateral deviations observed in the orchard pavement test.

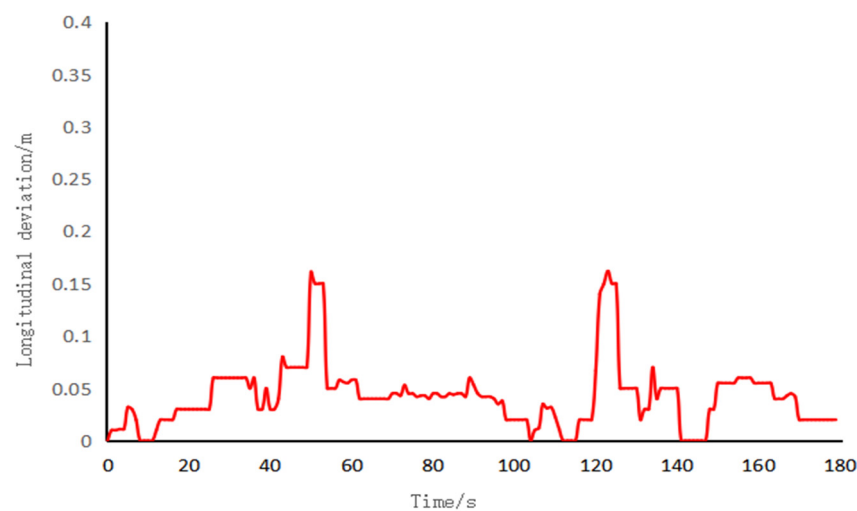


Figure 27. Longitudinal deviations observed in the orchard pavement test.

In this paper, the adaptive time domain MPC and fuzzy control algorithm are combined to establish a path-tracking controller to demonstrate the effectiveness of the path-tracking control strategy in an orchard environment, which is verified by field experiments. Considering the instability of the contact between the mowing robot and the surface of the orchard road, the next step can be used to analyze the constantly changing stress situation of the mowing robot wheel and design an advanced algorithm and a control strategy to improve the reliability of the drive anti-skid control.

5. Conclusions

This paper analyzes and establishes a kinematic model based on MPC for a four-wheel differential mowing robot. The complexity of the given orchard environment leads to excessive slippage by the driving wheel of the mower, which reduces the stability and accuracy of the path tracking of the lawn mower. A path-tracking controller is designed for the lawn mower that consists of an adaptive MPC, fuzzy control, and PID control, which can control the slip rate of the driving wheel to achieve anti-slip drive control.

1. The effectiveness of adaptive time domain MPC and traditional MPC path-tracking controller is compared in a MATLAB simulation. Compared with traditional MPC control, the adaptive time domain MPC path-tracking controller has an average lateral error absolute value that is 3.2 cm smaller and an average longitudinal error absolute value that is 1.7 cm smaller.
2. Simulation experiments are conducted on the designed path-tracking controller combined with anti-slip driving control. The results show that the path-tracking controller with anti-slip driving control added can effectively maintain the slip rate of the driving wheel within the designed target slip rate range on random road surfaces, with an amplitude close to 0.2. The path-tracking controller without an added anti-slip drive controller exhibits a significant change in the slip rate, reaching an amplitude of 0.5. At this time, the lawn mower experiences severe slipping on random road surfaces, which has a significant impact on the effectiveness of path tracking.
3. The field test results show that the lawn mower equipped with a combination of anti-slip drive control and adaptive MPC path tracking has a good effect on tracking the reference path. The average lateral error value can be controlled within approximately 5 cm, and the average longitudinal error value can be controlled within 4 cm. At the same time, the slip rate of the driving wheel can be maintained within the target slip rate range, indicating that the proposed controller can reduce the sliding of the driving wheel while ensuring high path-tracking accuracy.

Author Contributions: Conceptualization: J.L. and S.W.; methodology: J.L. and Y.C.; software: J.L. and S.W.; validation: J.L., S.W., W.Z. and H.L.; formal analysis: J.L., S.W. and H.L.; investigation: J.L.; resources: J.L. and Y.C.; data curation: S.W.; writing—original draft preparation: J.L., S.W., Y.C. and H.L.; writing—review and editing: J.L., S.W., T.W. and Y.Z.; visualization: S.W., R.J., C.M., X.Q. and K.F.; supervision: J.L. and Y.C.; project administration: J.L.; funding acquisition: J.L. All authors have read and agreed to the published version of the manuscript.

Funding: This work was supported by the Guangdong Laboratory for Lingnan Modern Agriculture under grants NZ2021040 and NZ2021009, the China Agriculture Research System under grant CARS-32, the Special Project of the Rural Vitalization Strategy of the Guangdong Academy of Agricultural Sciences under grant TS-1-4, and the Guangdong Provincial Modern Agricultural Industry Technology System under grant 2021KJ123.

Data Availability Statement: The data used to support the findings of this study are included within the article.

Conflicts of Interest: The authors declare no conflict of interest.

References

1. FAO (Food and Agriculture Organization of the United Nations). *Recommendations for Improved Weed Management*; Plant Production and Protection Division: Rome, Italy, 2006; pp. 1–56.
2. Nishimura, Y.; Yamaguchi, T. Grass Cutting Robot for Inclined Surfaces in Hilly and Mountainous Areas. *Sensors* **2023**, *23*, 528. [[CrossRef](#)] [[PubMed](#)]
3. Ding, Y.; Wang, L.; Li, Y.W.; Li, D.L. Model predictive control and its application in agriculture: A review. *Comput. Electron. Agric.* **2018**, *151*, 104–117. [[CrossRef](#)]
4. Chen, S.P.; Xiong, G.M.; Chen, H.Y.; Negrut, D. MPC-based path tracking with PID speed control for high-speed autonomous vehicles considering time-optimal travel. *J. Cent. South Univ.* **2020**, *27*, 3702–3720. [[CrossRef](#)]
5. Wang, Z.; Sun, K.; Ma, S.; Sun, L.; Gao, W.; Dong, Z. Improved Linear Quadratic Regulator Lateral Path Tracking Approach Based on a Real-Time Updated Algorithm with Fuzzy Control and Cosine Similarity for Autonomous Vehicles. *Electronics* **2022**, *11*, 3703. [[CrossRef](#)]
6. Zhang, C.; Gao, G.; Zhao, C.; Li, L.; Li, C.; Chen, X. Research on 4WS Agricultural Machine Path Tracking Algorithm Based on Fuzzy Control Pure Tracking Model. *Machines* **2022**, *10*, 597. [[CrossRef](#)]
7. Zhong, C.-Q.; Wang, L.; Xu, C.-F. Path Tracking of Permanent Magnet Synchronous Motor Using Fractional Order Fuzzy PID Controller. *Symmetry* **2021**, *13*, 1118. [[CrossRef](#)]
8. Jeong, Y.; Yim, S. Model Predictive Control-Based Integrated Path Tracking and Velocity Control for Autonomous Vehicle with Four-Wheel Independent Steering and Driving. *Electronics* **2021**, *10*, 2812. [[CrossRef](#)]

9. Fue, K.; Porter, W.; Barnes, E.; Li, C.; Rains, G. Autonomous Navigation of a Center-Articulated and Hydrostatic Transmission Rover using a Modified Pure Pursuit Algorithm in a Cotton Field. *Sensors* **2020**, *20*, 4412. [[CrossRef](#)]
10. Paramesh, S.; Suresh Rajendran, A. Unified seakeeping and manoeuvring model with a PID controller for path following of a KVLCC2 tanker in regular waves. *Appl. Ocean Res.* **2021**, *116*, 102860. [[CrossRef](#)]
11. Yang, Y.; Li, Y.K.; Wen, X.; Zhang, G.; Ma, Q.L.; Cheng, S.K.; Qi, J.; Xu, L.Y.; Chen, L.Q. An optimal goal point determination algorithm for automatic navigation of agricultural machinery: Improving the tracking accuracy of the Pure Pursuit algorithm. *Comput. Electron. Agric.* **2022**, *194*, 106760. [[CrossRef](#)]
12. Sun, C.Y.; Sun, P.; Zhou, J.; Mao, J. Travel Reduction Control of Distributed Drive Electric Agricultural Vehicles Based on Multi-Information Fusion. *Agriculture* **2022**, *12*, 70. [[CrossRef](#)]
13. Bai, G.; Meng, Y.; Liu, L.; Luo, W.; Gu, Q.; Liu, L. Review and Comparison of Path Tracking Based on Model Predictive Control. *Electronics* **2019**, *8*, 1077. [[CrossRef](#)]
14. Wu, H.; Zhang, H.; Feng, Y. MPC-Based Obstacle Avoidance Path Tracking Control for Distributed Drive Electric Vehicles. *World Electr. Veh. J.* **2022**, *13*, 221. [[CrossRef](#)]
15. Liu, G.H.; Zhang, H.; Zhang, D.; Shen, Y.; Wang, Z.J.; Xu, Y.D. High clearance four-wheel independent electric drive sprayer path tracking control based on self-correction controller. *J. Phys. Conf. Ser.* **2022**, *2383*, 012043. [[CrossRef](#)]
16. Xu, J.H.; Lai, J.; Guo, R.; Lu, X.; Xu, L. Efficiency-Oriented MPC Algorithm for Path Tracking in Autonomous Agricultural Machinery. *Agronomy* **2022**, *12*, 1662. [[CrossRef](#)]
17. Manikandan, S.; Kaliyaperumal, G.; Hakak, S.; Gadekallu, T.R. Curve-Aware Model Predictive Control (C-MPC) Trajectory Tracking for Automated Guided Vehicle (AGV) over On-Road, In-Door, and Agricultural-Land. *Sustainability* **2022**, *14*, 12021. [[CrossRef](#)]
18. He, J.; Hu, L.; Wang, P.; Liu, Y.X.; Man, Z.X.; Tu, T.P.; Yang, L.N.; Li, Y.Y.; Yi, Y.L.; Li, W.C.; et al. Path tracking control method and performance test based on agricultural machinery pose correction. *Comput. Electron. Agric.* **2022**, *200*, 107185. [[CrossRef](#)]
19. Huang, P.K.; Zhang, Z.G.; Luo, X.W.; Liu, Z.E.; Wang, H.; Yue, B.B.; Gao, W.W. Development of external acceleration identification and attitude estimation system of field working vehicle. *Trans. Chin. Soc. Agric. Eng.* **2019**, *35*, 9–15.
20. Ge, L.H.; Zhao, Y.; Ma, F.W.; Guo, K.H. Towards longitudinal and lateral coupling control of autonomous vehicles using offset free MPC. *Control Eng. Pract.* **2022**, *121*, 105074. [[CrossRef](#)]
21. Guo, J.C.; Shen, W.B.; Ning, J.S. Development of Lee's exact method for Gauss–Krüger projection. *J. Geod.* **2020**, *94*, 58. [[CrossRef](#)]
22. Liu, X.X.; Wang, W.; Li, X.L.; Liu, F.S.; He, Z.H.; Yao, Y.Z.; Ruan, H.P.; Zhang, T. MPC-based high-speed trajectory tracking for 4WIS robot. *ISA Trans.* **2022**, *123*, 413–424. [[CrossRef](#)] [[PubMed](#)]
23. Wang, W.R.; Yan, J.H.; Wang, H.; Ge, H.L.; Zhu, Z.Y.; Yang, G.J. Adaptive MPC trajectory tracking for AUV based on Laguerre function. *Ocean Eng.* **2022**, *261*, 111870. [[CrossRef](#)]
24. Goncalo, C.P.; Wahlberg, B.; Pettersson, H.; Martensson, J. Adaptive reference aware MPC for lateral control of autonomous vehicles. *Control Eng. Pract.* **2023**, *132*, 105403. [[CrossRef](#)]
25. Guan, L.; Liao, P.; Wang, A.; Shi, L.; Zhang, C.; Wu, X. Path tracking control of intelligent vehicles via a speed-adaptive MPC for a curved lane with varying curvature. *Proc. Inst. Mech. Eng. Part D J. Automob. Eng.* **2022**, 09544070221133967. [[CrossRef](#)]
26. Pacejka, H.B. *Tire and Vehicle Dynamics*; Elsevier: Oxford, UK, 2012.
27. Juan, C.; Javier, P. A Procedure for Determining Tire-Road Friction Characteristics Using a Modification of the Magic Formula Based on Experimental Results. *Sensors* **2018**, *18*, 896.
28. Bakker, G.E.; Pacejka, H.B.; Lidner, L. A New Tire Model with an Application in Vehicle Dynamics Studies. *SAE Paper* **1989**, *98*, 101–113.
29. Yang, S.; Feng, J.; Song, B. Research on Decoupled Optimal Control of Straight-Line Driving Stability of Electric Vehicles Driven by Four-Wheel Hub Motors. *Energies* **2021**, *14*, 5766. [[CrossRef](#)]
30. Stephen, B.J.; Emmanuel, G.D.; Afeez, A.; David, O.O.; Ban, M.K. Metaheuristic algorithms for PID controller parameters tuning: Review, approaches, and, open problems. *Heliyon* **2022**, *8*, e09399. [[CrossRef](#)]

Disclaimer/Publisher's Note: The statements, opinions and data contained in all publications are solely those of the individual author(s) and contributor(s) and not of MDPI and/or the editor(s). MDPI and/or the editor(s) disclaim responsibility for any injury to people or property resulting from any ideas, methods, instructions or products referred to in the content.